JOURNAL OF GUIDANCE, CONTROL, AND DYNAMICS
Vol. 31, No. 3, May–June 2008

Optimal Lunar Launch Trajectories to the Sun–Earth L1 Vicinity

Keith Jackson* and Victoria L. Coverstone†
University of Illinois at Urbana–Champaign, Urbana, Illinois 61801

DOI: 10.2514/1.30877

The sun/Earth–moon L1 point is a growing target for space missions. This paper assumes a need to place an object directly between the Earth and the sun. Possible purposes for such a mission include a type of shield to intercept some portion of the sun's rays, or conversely a lens or mirror to focus them. In addition, this paper requires a launch directly from the moon instead of a traditional orbit-to-orbit transfer. A detailed case using accurate positional and velocity data for all planetary bodies is used in this paper. Instead of focusing solely on trajectories defined as optimal by minimum fuel consumption, we looked for trajectories with low sensitivity to initial conditions to additionally minimize the frequency and magnitude of course corrections. We first analyzed the reverse problem to identify solution areas of low sensitivity to launch conditions. Using the determined restricted solution space, we were successfully able to determine a launch site on the moon that could reach L1 with the greatest number of low-cost trajectories and launch windows within the resolution of the solution space.

Introduction

AS AN equilibrium point sitting directly between the Earth and the sun, the first Lagrange point (L1) is of great interest to mission planners despite its instability. In the last 30 years, several missions have made the journey to and maintained orbits about L1 to better study various features of the solar system. However, all prior missions to L1 so far have left from the Earth and entered a wide orbit about L1 that kept the spacecraft out of the direct line between the Earth and the sun for communication purposes. This paper uses a different approach—the spacecraft is assumed to be manufactured on the moon, it is launched from the moon via a ballistic method, and it either enters a small-amplitude orbit about L1 or maintains its position in the vicinity of L1, thus remaining within the direct line between the Earth and the sun 100% of the time.

There are many motivations for these differences. First, the moon has a much shallower gravity well than the Earth and so the fuel costs for launching from the moon will be much lower than for launching from the Earth. Also, the lack of atmosphere on the moon eliminates the need for a heat shield and allows all of the impulse to be imparted to the spacecraft immediately at launch. A ballistic (impulsive) launch was studied as a more efficient method of launching the spacecraft, negating the need to provide extra power for lifting additional launch fuel and tanks and reducing the magnitude of the launch impulse velocity to a secondary cost. Finally, a trajectory that places the spacecraft close enough to L1 to remain long term directly between the Earth and the sun was sought in order to design missions that directly make use of this location—mainly some form of interference with the sun's rays before they reach the Earth, either in the form of a shield that could partially block the sun or a mirror or lens that could redirect or focus the rays. Obviously this is a future-oriented concept because it assumes both the ability to use materials already present on the moon to manufacture the spacecraft and the need to in some way interfere with the sun's rays. One such future need for blocking the sun's rays would be to counteract the effects of global warming, as described by Angel [1].

The problem of identifying optimal trajectories from the moon to L1 is not as simple as determining the single trajectory with the lowest fuel cost or transfer time. Presumably, the ballistic launch method would allow for a freely changeable impulse direction and magnitude, whereas the launch site would likely be immobile and fixed. The launch windows should also have maximum duration and frequency, though the specific timing is not truly a concern. In addition the trajectory must be relatively insensitive to initial conditions to minimize the hidden costs of course corrections. Thus this paper will focus on determining a launch site on the moon that provides the longest and most frequent launch windows for trajectories to L1 that minimize, in turn, sensitivity to initial conditions, quantity of fuel spent during flight and upon arrival at L1 (proportional to the sum of the impulse magnitudes), transfer time between the moon and L1, and resources consumed during the ballistic launch from the moon (again proportional to the impulse magnitude).

Several spacecraft have been sent to L1 in the past few decades to take advantage of the point's unique properties. The International Sun/Earth Explorer 3 (ISEE-3) became the first spacecraft to be stationed in an orbit about a Lagrange point in November 1978 when it arrived in a Halo orbit about the sun/Earth–moon L1 point. Its mission was to study the interplanetary space upstream from Earth [2].

The Solar and Heliospheric Observatory (SOHO) arrived at a Halo orbit about L1 in March 1996 and remains there to this day. As its name implies, SOHO's mission was to sit 1.5×10^6 km closer to the sun than to the Earth, and observe the sun as closely as possible [3].

The Advanced Composition Explorer (ACE) is the third spacecraft to enter an orbit about a Lagrange point, launching in August 1997. ACE made use of the sun/Earth–moon L1 point to get away from the interference caused by the Earth's magnetic field yet still maintain a stable position relative to the Earth. The primary mission for the ACE spacecraft was to observe and study the composition of the interplanetary medium, the interstellar medium, galactic matter, and the solar corona [4].

In September 2004, the Genesis spacecraft became the first mission to return to Earth from the sun/Earth–moon L1 point. Genesis arrived at L1 in November 2001 and collected samples of the solar wind for 2.5 years before leaving to return to Earth. Upon its return to Earth in 2004, the Genesis capsule was supposed to be picked up midair, but its parachute failed to deploy and it crashed into the ground. Fortunately the solar collectors were in excellent shape and the analysis of the returned data continues [5].

These missions have clearly demonstrated the capability to send a spacecraft to L1 and have it remain there for long periods of time. The station-keeping costs are generally minimal compared to the costs of attitude control or orbit insertion for these Earth-launched missions

Received 7 March 2007; revision received 14 August 2007; accepted for publication 24 August 2007.

*Research Assistant, Department of Aerospace Engineering, 306 Talbot Lab, 104 South Wright Street.

†Professor, Department of Aerospace Engineering, 306 Talbot Lab, 104 South Wright Street.

to large-amplitude orbits about L1. For the mission considered in this paper, however, a spacecraft leaves directly from the moon and either enters a small-amplitude Lissajous orbit about L1 or sits directly at L1 itself to remain directly within the sun–Earth cone. A second spacecraft in a Halo orbit will likely be required in order to maintain communications with the first, if necessary.

Theory

Reference Frames

For an n-body problem, the gravitational acceleration of a spacecraft is defined by summing up the forces due to each of the bodies using Newton's law of gravitation [6]:

$$\ddot{\mathbf{R}} = -\sum_{j=1}^{n-1} \frac{Gm_j}{r_j^3}\mathbf{r}_j \tag{1}$$

In Eq. (1), m_j = mass of jth body, G = universal gravitational constant, $\mathbf{r}_j$ = position vector from jth body to spacecraft, r_j = magnitude of $\mathbf{r}_j$, and $\mathbf{R}$ = position vector from origin to spacecraft. It is assumed that the spacecraft is the nth body.

For this paper, five bodies are considered: the sun, the Earth, the moon, the Jupiter system (for disturbance purposes only), and the spacecraft. Hereafter, the subscripts 1–4 will refer to the first four bodies listed unless otherwise noted, whereas a lack of a subscript indicates that the variable refers to the spacecraft.

To expedite analysis of the problem, four reference frames have been defined. A full explanation of each reference frame is as follows:

The first reference frame is fixed with the sun as its origin, with the x axis coinciding with the intersection of the Earth's equatorial plane with the ecliptic plane on 1 January 2000 (J2000), the y axis forming a plane with the x axis parallel to the Earth's equatorial plane on J2000, and the z axis forming a right-hand system with the other two axes.

The second reference frame, often called the geocentric solar ecliptic (GSE) system, is centered on the Earth and rotates so that the x' axis points away from the sun, the z' axis is parallel to the angular momentum vector of the Earth's orbit about the sun, and the y' axis again forms a right-hand system. The angle υ, the declination, is defined as the angle between the x' axis and the xy plane, while the angle λ, the right ascension, is the angle between the x'-axis's projection into the xy plane and the x axis.

The third reference frame is centered on the moon and rotates so that the x'' axis points away from the Earth, the y'' axis forms an $x''y''$ plane that is parallel to the moon's orbital plane, and the z'' axis is parallel to the angular momentum vector of the moon's orbit about the Earth. The angles η and φ are defined in the same manner as υ and λ, respectively; η is the ecliptic latitude, the angle between the x'' axis and the $x'y'$ plane, while φ is the ecliptic longitude, the angle between the x''-axis's projection down to the $x'y'$ plane and the x' axis. In terms of the moon's phases, $\varphi = 0$ deg would indicate a full moon, $\varphi = 90$ deg is last quarter, $\varphi = 180$ deg is new moon, and $\varphi = 270$ deg is first quarter.

The fourth reference frame is centered on the spacecraft's launch point on the surface of the moon, and again rotates with time so that the x''' axis points directly upward from the moon's surface, and the y''' and z''' axes point toward local east and north, respectively, in the horizon, at the launch position of the spacecraft. The two angles ψ and θ correspond roughly to the selenographic latitude and longitude, respectively, with differences of up to 8 deg due to lunar librations. Once again, ψ is defined in the same manner as η and υ—it is the angle between the x''' axis and the $x''y''$ plane. Also, like φ and λ, θ is the angle between the x'''-axis's projection to the $x''y''$ plane and the x'' axis. With these definitions, the center of the face of the moon seen from the Earth corresponds to $\theta = 180$ deg and $\psi = 0$ deg.

Two other angles are used within the fourth reference frame to define the direction of the launch impulse. Both angles are defined in the same manner as the previous three sets—β is the angle between the impulse vector ($\Delta\mathbf{v}$) and the $x'''y'''$ plane, and α is the angle between $\Delta\mathbf{v}$'s projection into the $x'''y'''$ plane and the x''' axis.

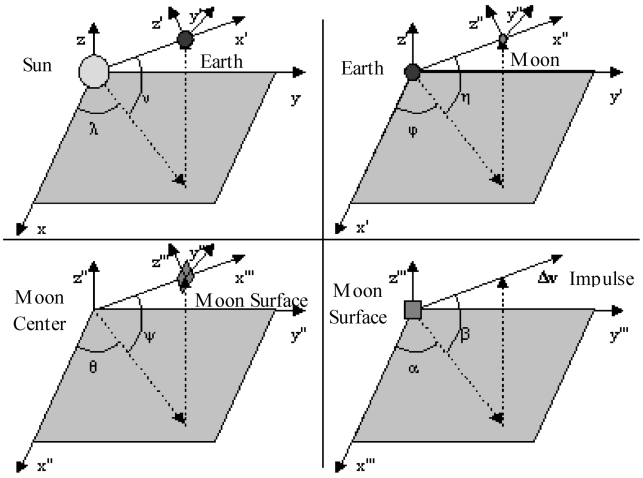

Fig. 1 Illustration of reference frames and angles.

Although the more conventional angles azimuth and elevation could have been used in this case, these definitions for α and β were used to remain consistent with the other coordinate system angles.

Figure 1 illustrates the definition of each reference frame and of the various angles relating them.

Henceforth, a superscript in parentheses will be used to show in which reference frame a variable is defined, unless it refers to the first reference frame in which case no superscript will be used. Of the angles shown in Fig. 1, only those from the first two reference frames —λ, υ, φ, and η—are functions of time, because they depend on the position of the Earth and the moon. The angles in the third and fourth reference frames—θ, ψ, α, and β—depend only on the spacecraft's launch conditions and so have a single value for the launch time.

All calculations using the equations of motion were performed in the first reference frame. The fourth reference frame is only used to define the launch $\Delta\mathbf{v}$ of the spacecraft. The third reference frame, besides being used to define the fourth reference frame, is used primarily to easily define the launch position of the spacecraft in terms of its position on the moon's surface. It is also used to calculate the velocity imparted to the spacecraft due to the moon's rotation. The second reference frame, in addition to defining subsequent frames, is used extensively to plot the paths of the spacecraft and the moon in the Earth system.

Model Formulation

The model used for this paper calculated a set of initial conditions and integrated them forward in time. The orbits of the Earth and the moon are accurately modeled as slightly elliptical and not coplanar, and all of the angles of Fig. 1 are free to take on any value. In addition, the model includes disturbance effects of the Jupiter system. This problem requires optimizing six parameters that define the spacecraft's initial position and velocity: initial time T, θ, ψ, α, β, and Δv. The position and velocity vectors for the Earth, the moon, and the Jupiter system barycenter were obtained from the Jet Propulsion Laboratory's Horizons database [7]. Data points were taken for every 12 h from 1 January 2020 through 31 December 2030, and pregenerated cubic splines were used in the model to interpolate between these data points during the integration process for those time steps immediately after launching from the moon's surface, as the close proximity to the moon required time steps much smaller than the available ephemeris data.

The variables λ, υ, φ, and η are defined by the launch time T using the Horizons data for the moon, $\mathbf{R}_3(t)$, $\mathbf{V}_3(t)$ at $t = T$ and basic trigonometric equations and coordinate transforms between the reference frames. Then Eqs. (2) and (3), along with coordinate transforms between the appropriate reference frames, define $\mathbf{R}(T)$ and $\mathbf{V}(T)$ for the spacecraft:

$$\mathbf{R}^{(3)}(T) = \mathbf{R}_3^{(3)}(T) + \rho_3 \begin{bmatrix} \cos\theta\cos\psi \\ \sin\theta\cos\psi \\ \sin\psi \end{bmatrix} \tag{2}$$

Table 1 Parameter values for 3-D model

Parameter	Description	Value
ρ_3	Average radius of moon	1737.53 km
ω_3	Average rotational velocity of moon	2.6617e − 6 rad/s
$\mu_1 = Gm_1$	Gravitational constant of sun	1.3271e + 11 km^3/s^2
$\mu_2 = Gm_2$	Gravitational constant of Earth	398, 600 km^3/s^2
$\mu_3 = Gm_3$	Gravitational constant of moon	4902.8 km^3/s^2
$\mu_4 = Gm_4$	Gravitational constant of Jupiter system	1.2671e + 8 km^3/s^2
ρ	Average fractional distance between Earth and L1	0.010078

$$\mathbf{V}^{(4)}(T) = \mathbf{V}_3^{(4)}(T) + \begin{bmatrix} \Delta v \cos\alpha \cos\beta \\ \rho_3\omega_3 \cos\psi + \Delta v \sin\alpha \cos\beta \\ \Delta v \sin\beta \end{bmatrix} \quad (3)$$

Note that in Eqs. (2) and (3), the variables ρ_3 and ω_3 represent the average values for the moon's radius and its rotational velocity, respectively.

MATLAB's ode113 integration routine [8] was used to integrate these initial conditions using Eq. (1) and the Horizons data defining $\mathbf{R}_2(t)$, $\mathbf{R}_3(t)$, and $\mathbf{R}_4(t)$. With the relatively large accelerations close to the moon's surface, a very small initial time step of 1e − 9 s was used, with a maximum time step of 1e + 5 s used when the solution satisfied absolute and relative tolerances of 1e − 12. The ode113 routine was chosen because it provided slightly more accurate solutions close to the moon's surface and a faster computation time. The constants of Eqs. (1–3), obtained from the Horizons data, are listed in Table 1.

This problem is a six-parameter optimization problem, with the primary fitness function equal to the inverse of the terminal impulse required to keep the spacecraft at L1 upon its arrival. Secondary fitness values examined include the inverse of the transfer time and the inverse of the sensitivity of the trajectory to launch conditions. The model would stop running and assign a fitness value of zero if the spacecraft crashed into either the moon or the Earth, moved more than 0.04 astronomical units (AU) away from the Earth, or remained in the Earth system for more than 10 years without reaching L1.

One way to further simplify the problem is to solve it in reverse: With the spacecraft starting at L1, find optimal trajectories that reach the moon. There are several reasons why this problem is easier to solve. First, finding a trajectory that reaches the moon is much easier than finding a trajectory that reaches L1 because the moon's gravity well will help pull in any spacecraft that approaches. In addition, launching from a point (L1) requires two fewer parameters than launching from a sphere (the moon), because we do not need to define our position on L1 using the equivalent of θ and ψ. Finally, when launching from L1 we are free to choose a minimal Δv imparted to the spacecraft at L1, simultaneously eliminating an optimization parameter and simplifying the fitness function. The actual value for Δv chosen will be the minimum value which provides a large variety of possible trial solutions, as described in the next section.

We are left with three parameters to optimize: two angles representing the direction of $\mathbf{\Delta v}$, and the launch time T. The two angles, δ and γ, are defined in a manner similar to the angles of Fig. 1: δ is the angle between the x' axis and the projection of $\mathbf{\Delta v}$ into the $x'y'$ plane, and γ is the angle between $\mathbf{\Delta v}$ and the $x'y'$ plane. Thus by reversing the problem, we reduce the number of parameters to optimize from six to three. Because there is no air resistance on the moon, there are no losses in the system and any trajectory found with the reverse models will be completely reversible. Thus we can find those trajectories that reach the moon from L1, and choose those that have the lowest Δv at the moon and the shortest transfer time.

The positions of the bodies in the reverse model are the same as their forward counterparts. The reverse model has initial conditions as defined in Eq. (4), after appropriate coordinate transforms:

$$\mathbf{R}(T) = (1-\rho)\mathbf{R}_2(T)$$
$$\mathbf{V}^{(2)}(T) = (1-\rho)\mathbf{V}_2^{(2)}(T) + \Delta\mathbf{v}[\cos\delta\cos\gamma \quad \sin\delta\cos\gamma \quad \sin\gamma]^T \quad (4)$$

The constants in Eq. (4) have the same values as in Table 1. The problem is solved in reverse time, that is, from "starting" time T to "final" time t_f such that $t_f < T$, so that when the trajectory is reversed it is in normal time. Because the spacecraft does not start near a gravity well in this case, the initial step does not need to be as small, and so the default value of 1e − 3 s was used. The maximum time step was again 1e + 5 s, though the tolerances did not need to be as tight so were set at 1e − 6 for both relative and absolute tolerances. For this paper, the reverse problem was solved first and the results from the reverse model were used to identify optimal narrow bands for the parameters of the forward model. The forward model was then run within these bands to identify the optimal launch window and launch site location.

Results and Discussion

Reverse Model

The first scenario analyzed, referred to as case 1, was used to narrow the range of parameters tested. The moon's gravity was lumped in with that of the Earth, and a grid of initial conditions was tested to see which portion of the (δ, γ, Δv) space would allow the spacecraft to intercept the moon's orbit. Refer to Fig. 1 and the previous section for definitions of the variables. Figure 2 shows a three-dimensional scatter plot of those sets of initial conditions that successfully reached the moon's orbit.

In Fig. 2, the shading is based on the magnitude of the relative velocity between the spacecraft and the moon when the spacecraft intercepts the moon's orbit, assuming the moon were present at the interception point. The dark regions represent larger magnitudes and the light regions represent smaller ones.

For subsequent simulations, we can now choose Δv = 10 m/s as a relatively low value that still provides a large number of different trial solutions. We then restrict δ and γ using Fig. 2. Before proceeding with the full reverse run, the effects of the launch time T were examined: case 2 fixed $\delta = 0$ deg, $\gamma = 0$ deg, and Δv = 10 m/s and tested values of T every 12 h from 1 January 2020 through 31 December 2030. Those conditions that successfully reached the moon were given a fitness value of the reciprocal of the impact velocity on the moon, Δv_{end}; otherwise the fitness value was set to zero. Figure 3 shows a scatter plot of the fitness values vs the launch time for all of the trial solutions, along with a lighter fixed horizontal line showing the successful launch times.

Most of the solutions have an impact velocity around 2.35–2.4 km/s, near the escape velocity of the moon, with a smaller cluster of solutions having impact velocities near 2.45–2.5 km/s. The data in Fig. 3 indicate that any given 2-year

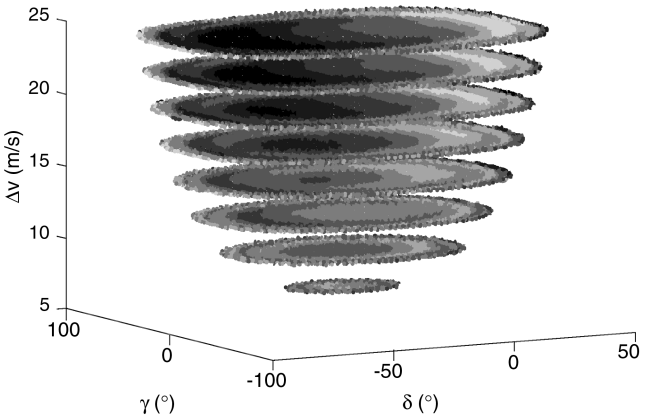

Fig. 2 Portion of the (δ, γ, Δv) space that allows the spacecraft to intercept the moon's orbit for case 1.

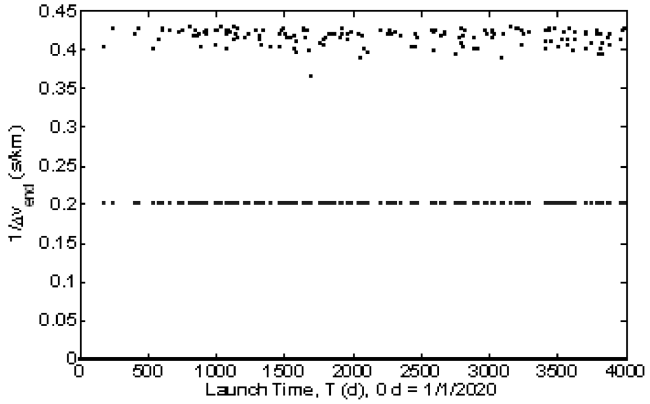

Fig. 3 Fitness values vs T for case 2. Horizontal line shows successful solutions vs T with fitness value fixed to 0.2.

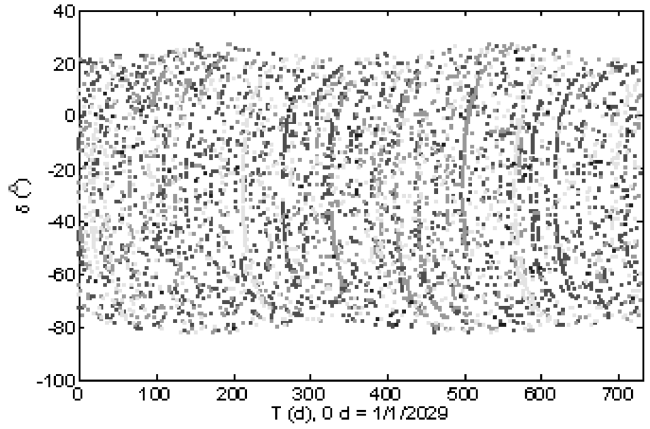

Fig. 4 Shaded plot of (T, δ) space for successful solutions of case 3.

window in this range should have a satisfactory number of successful solutions, because there are no long gaps or concentrations.

For the full reverse simulation, T was restricted to values every 12 h from 1 January 2029 through 31 December 2030. As mentioned previously, the launch impulse was chosen to be $\Delta v = 10$ m/s. Because the moon has only small oscillations in the z' direction compared to the distance the spacecraft travels in the $x'y'$ plane to reach the moon from L1, it was discovered that for small Δv and small γ, the spacecraft's motions in the z' direction and in the $x'y'$ plane were nearly independent, with γ only affecting motion in the z' direction and δ only affecting motion in the $x'y'$ plane. Thus the full reverse simulation was split into two pieces. In the first, case 3 fixed $\gamma = 0$ and used Fig. 2 to find the range of δ values that could be used for $\Delta v = 10$ m/s. Thus case 3 tested a grid of just two parameters: T every 12 h from 1 January 2029 through 31 December 2030, and δ every 0.5 deg from -90 deg through 40 deg. In addition, the maximum transfer time was limited to 2 years.

Figure 4 shows a shaded scatter plot of the successful solutions in the (T, δ) space. The darkest points correspond to Δv_{end} values between 2.33 and 2.37 km/s, the medium points correspond to Δv_{end} values between 2.37 and 2.45 km/s, and the lightest points correspond to Δv_{end} values between 2.45 and 2.55 km/s.

Figure 4 is consistent with Fig. 2, with most of the successful solutions having impact velocities from 2.33 to 2.45 km/s. So once again we see that it should be possible to reach L1 from the moon with a launch velocity just equaling escape velocity and minimal impulse required upon arrival at L1. In Fig. 4, families of solutions can be seen with parabolic forms that have vertices near $\delta = -28.5$ deg and slightly increase in T as δ is moved from this value. To see if these families of solutions have corresponding clusters in the landing conditions on the moon, Fig. 5 plots ψ vs θ, t_f vs θ, and t_f vs ψ, respectively, for successful solutions, with each figure shaded in the same manner as in Fig. 4.

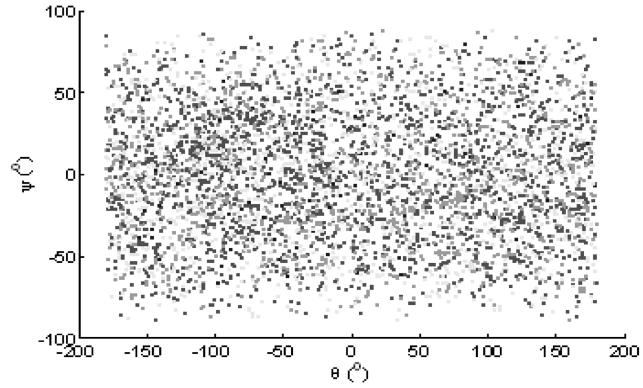

a) ψ vs θ

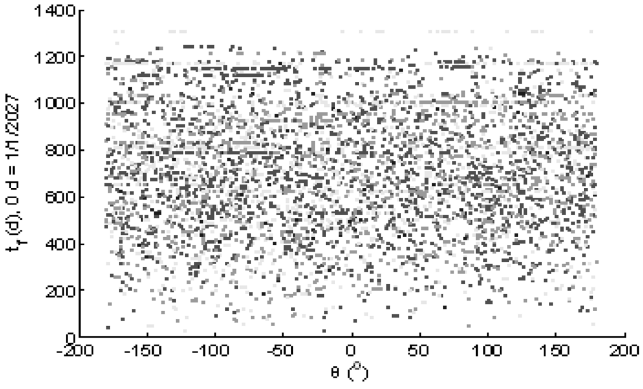

b) t_f vs θ

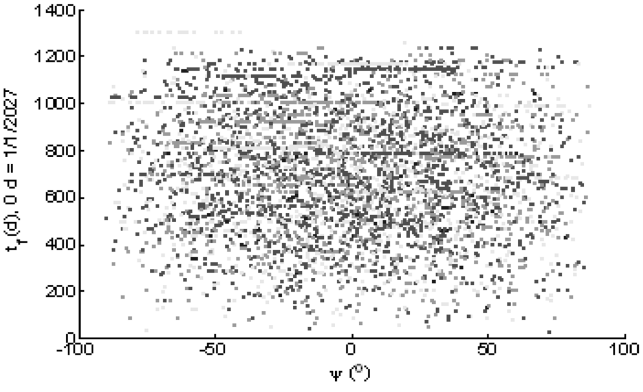

c) t_f vs ψ

Fig. 5 Shaded plot of (ψ, t_f) space for successful solutions of case 3.

Although the scatter in Fig. 5a does not seem to indicate any patterns, the horizontal lines in Figs. 5b and 5c indicate that the families of solutions of Fig. 4 have a near-uniform t_f within each family. Thus the parabolic shape of the families of Fig. 4 suggests that the spacecraft reaches the moon more quickly if δ is farther from the -28.5 deg value marking the centerline of Fig. 2. To make sure that the constraint of $\Delta t < 2$ years did not excessively restrict the problem, Fig. 6 plots Δv_{end} vs Δt for the successful solutions.

Figure 6 shows a cluster of fast-transfer solutions near $\Delta v_{end} = 2.5$ km/s and $\Delta t = 130$ days, and a cluster of slow-transfer solutions near $\Delta v_{end} = 2.35$ km/s and $\Delta t = 200$ days. The data in Fig. 6 extend uniformly for larger Δt, indicating solutions with additional orbits about the Earth before impacting the moon. Because the primary solutions of interest are the lower Δt solutions associated with fewer Earth orbits, and these occur mainly for $\Delta t < 1$ year, the constraint of $\Delta t < 2$ years does not seem unduly restrictive.

The second piece of the full reverse simulation increases the variety of successful solutions by removing the restriction on γ. Case 4 takes each successful (T, δ) pair from case 3, and tests γ values

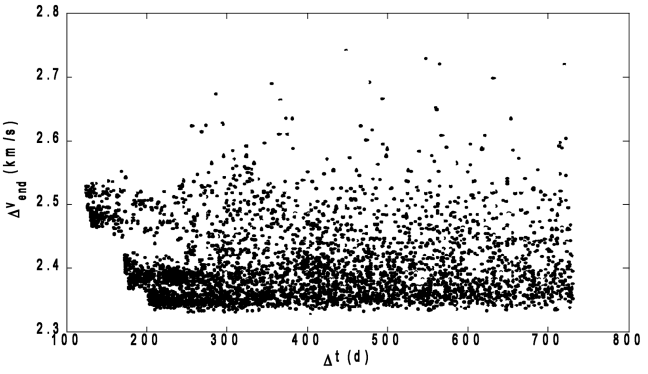

Fig. 6 Δv_{end} vs Δt for the successful solutions of case 3.

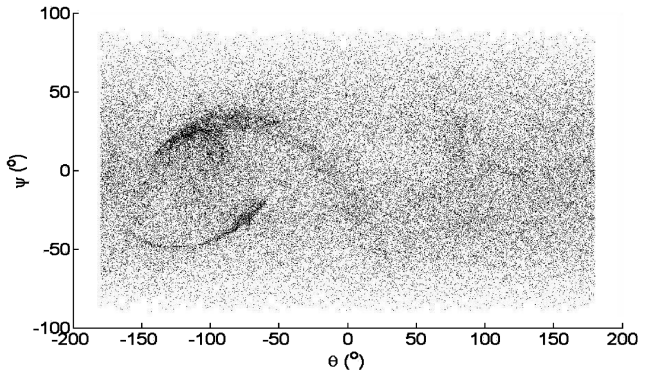

Fig. 7 ψ vs θ for successful solutions of case 4.

every 1 deg from −60 deg to 60 deg. For each trial solution in case 4, Δv is fixed so that the projected component in the $x'y'$ plane is always 10 m/s. Once again, the transfer time is restricted so that $\Delta t < 2$ years. With these parameters, each trial solution in case 4 should have approximately the same motion in the $x'y'$ plane as the corresponding successful solution of case 3. Figure 7 plots ψ vs θ for the successful solutions in an attempt to locate the point where the solutions are densest.

The data in Fig. 7 are dense everywhere, making it difficult to pinpoint a single focus region. There seems to be a structure in the left half of Fig. 7 resembling a hurricane, while the right half of Fig. 7 contains a large rectangular dense region. We will have to reexamine the data upon choosing the optimal launch windows. Remembering the horizontal lines of constant t_f in Fig. 5, Fig. 8 shows a histogram for t_f for the successful solutions of case 4.

There are several discrete spikes in Fig. 8 corresponding to the horizontal lines of Fig. 5. The locations of these spikes identify the optimal values for t_f and thus the optimal launch windows. Table 2 lists the launch windows (L.W.s) representing the tallest 16 spikes of Fig. 8.

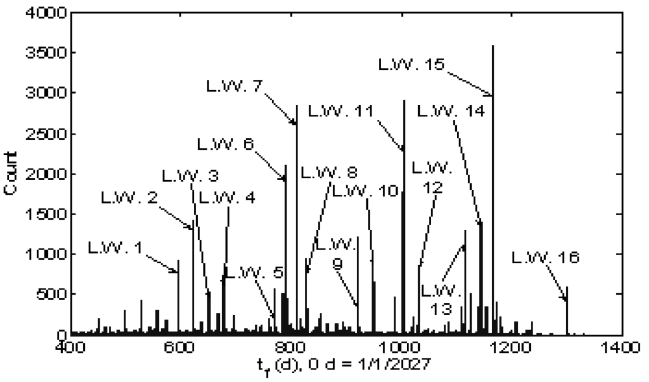

Fig. 8 Histogram for t_f for successful solutions of case 4.

Table 2 Date ranges for launch windows (L.W.S) of Fig. 8

L.W.	Start	End
1	7/18/2028 0:00	7/19/2028 12:00
2	9/12/2028 0:00	9/14/2028 12:00
3	9/30/2028 12:00	10/3/2028 0:00
4	10/27/2028 12:00	10/31/2028 0:00
5	2/7/2029 12:00	2/9/2029 0:00
6	2/26/2029 0:00	3/2/2029 12:00
7	3/31/2029 0:00	4/2/2029 0:00
8	4/15/2029 0:00	4/18/2029 0:00
9	7/8/2029 0:00	7/11/2029 0:00
10	8/4/2029 0:00	8/8/2029 0:00
11	9/28/2029 0:00	10/2/2029 0:00
12	10/26/2029 0:00	10/28/2029 0:00
13	1/17/2030 0:00	1/21/2030 0:00
14	2/15/2030 0:00	2/19/2030 0:00
15	3/9/2030 12:00	3/11/2030 0:00
16	7/24/2030 0:00	7/24/2030 12:00

From Table 2, the optimal launch windows occur anywhere from 3 weeks to 3 months apart and are each 1–4 days long. Upon selection of a focus region for the (θ, ψ) space we will return to these launch windows and eliminate some of them. To obtain a finer definition for Fig. 7, we can divide the (θ, ψ) space up into small square 5 deg-wide "bins" and count the number of times at least one point of Fig. 7 in each launch window falls in each bin. Thus each bin will have a value from zero up to a maximum of 16. Figure 9 shows the results in a surface histogram.

The dark points along the top and bottom of Fig. 9 represent a presence in 0–4 launch windows for that bin. The medium-gray points represent a presence in 5–8 launch windows, and the lightest points in the middle represent a presence in 9–12 launch windows. The black box highlights the selected focus region for this case, corresponding to θ between −125 deg and −105 deg and ψ between −20 deg and 0 deg. This region is centered on the trailing near side of the moon, 65 deg from the near side center and 10 deg south of the lunar equator. Note how this focus region also corresponds to the eye of the hurricanelike structure in Fig. 7 mentioned previously.

By concentrating on this small portion of the (θ, ψ) space, we can eliminate some of the launch windows of Table 2 from consideration. Even in the dark center regions of Fig. 9, there were no bins that had a presence in all 16 launch windows, so we expect that at least a few of the launch windows will not be represented in the focus region. Indeed, L.W.s 1, 2, 5, 9, and 16 had no presence in the focus region at all, and L.W.s 8 and 10 had such a small presence that they were excluded as well. Now we must define narrow ranges for the other input parameters for the forward model: α, β, and Δv. Because the magnitude and direction of the launch impulse from the moon can be easily changed, it is not necessary to force all launch windows to use the same range of values, as was the case for θ and ψ. Figure 10 plots

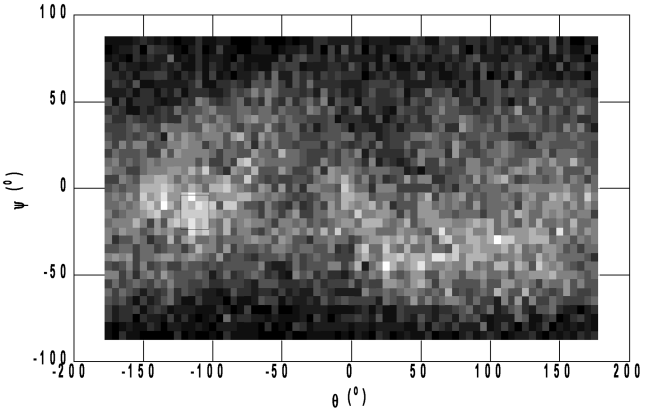

Fig. 9 Surface histogram of presence of (θ, ψ) points in each L.W. of Table 2.

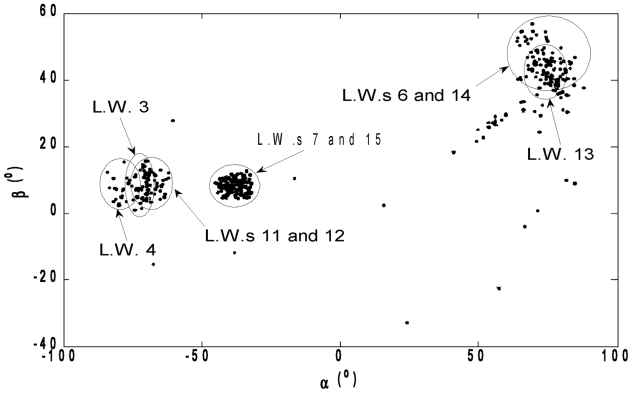

a) β vs α

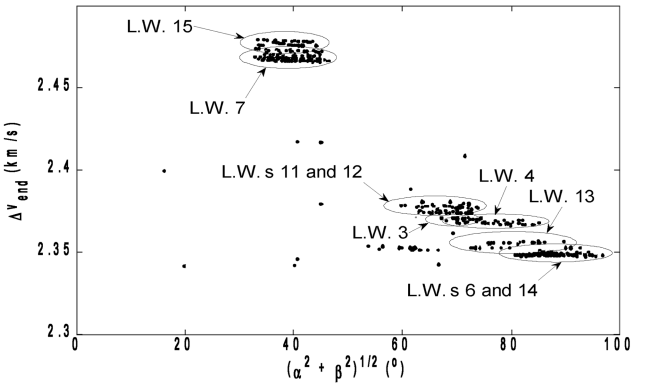

b) Δv vs $(\alpha^2 + \beta^2)^{1/2}$

Fig. 10 Plots of landing parameters for successful solutions of case 4, located inside the focus region of Fig. 19, for various L.W.s of Table 2.

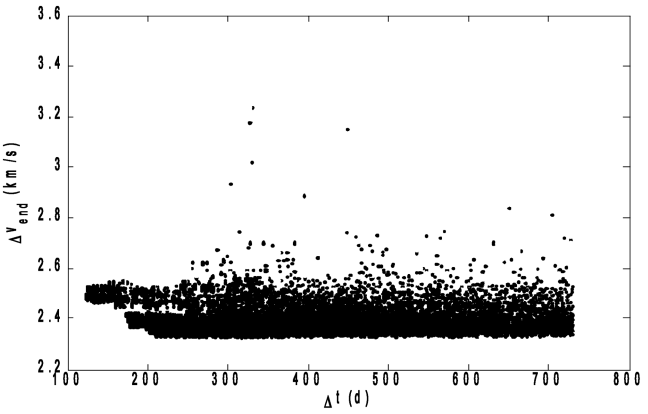

Fig. 11 Δv_{end} vs Δt for successful solutions of case 4.

β vs α and Δv vs $(\alpha^2 + \beta^2)^{1/2}$ for those successful solutions within the focus region of Fig. 9.

Because , in general, Fig. 10 shows that the launch windows have separate clusters of solutions, it is fortunate that we do not need a single range of values that applies to all launch windows. Notice how L.W.s 6 and 14, and 7 and 15, are nearly indistinguishable from each other. It is no coincidence that these pairs of L.W.s are almost exactly a year apart and thus are repeating the same conditions. This repetition helps to justify our decision to limit the tested launch times to a 2-year window, because it seems at least some of the solution families repeat each year.

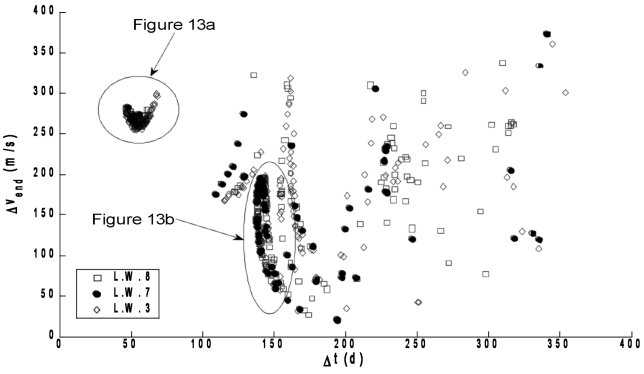

Fig. 12 Δv_{end} vs Δt for case 5, all successful solutions.

The final parameter to check is, again, the transfer time Δt. Judging by the previous analyses, we expect Δt to be less than a year for most cases, with fast-transfer solutions and slow-transfer solutions. Figure 11 plots Δv_{end} vs Δt for all successful solutions of case 4.

Figure 11 show results for case 4 that are comparable to those found in Fig. 6 for case 3 and that match our prior expectations. There is a region of fast-transfer solutions around $\Delta t = 150$ days and $\Delta v_{end} = 2.5$ km/s, and a region of slow-transfer solutions around $\Delta t = 225$ days and $\Delta v_{end} = 2.35$ km/s. Also notice that once again most solutions have a Δv_{end} between 2.33 and 2.55 km/s.

Forward Model

The combined results of Table 2 and Figs. 9–11 were used to define a narrow region of inputs for use with the forward model, shown in Table 3.

In Table 3, the L.W.s have been reindexed from Table 2, and the values for T are baselined so that $T = 0$ days refers to 1 January 2027. The angles in Table 3 used 4 deg increments, while the launch time used a 0.5 day increment and the launch impulse used a 2 m/s increment. Despite the reduced range of parameters obtained from the reverse model, the increments are still quite large due to the high number of parameters for the forward model. Case 5 uses the forward model and tests nine separate 6-parameter grids using the values in Table 3. A successful solution for case 5 is one where the spacecraft closes to within 15,000 km of L1. Figure 12 plots Δv_{end} vs Δt for all of these successful solutions.

As expected, Fig. 12 shows a dense cluster of fast-transfer solutions near $\Delta t = 55$ days and $\Delta v_{end} = 275$ m/s. Figure 12 also shows multiple slow-transfer curves near $\Delta t = 160$ days and Δv_{end} from 25 to 200 m/s. One final fact to notice is that once again the vast majority of successful solutions reached L1 in under 1 year, proving our limitation of 2 years on Δt to be a reasonable one.

Table 3 Ranges for input parameters for forward model

L.W.	T, day	θ, deg	ψ, deg	α, deg	β, deg	Δv, km/s
1	649.5:652	−125: − 105	−20:0	−79: − 68	0:16	2.368:2.372
2	676.5:680	−125: − 105	−20:0	−85: − 74	0:16	2.366:2.370
3	788:792.5	−125: − 105	−20:0	65:88	30:57	2.347:2.353
4	811:813	−125: − 105	−20:0	−46: − 32	4:13	2.466:2.472
5	1002:1006	−125: − 105	−20:0	−75: − 62	1:16	2.374:2.376
6	1030:1032	−125: − 105	−20:0	−75: − 62	1:16	2.375:2.381
7	1113:1117	−125: − 105	−20:0	−64: − 77	29:55	2.352:2.357
8	1142:1146	−125: − 105	−20:0	−65: − 88	30:57	2.347:2.353
9	1164.5:1166	−125: − 105	−20:0	−46: − 32	4:13	2.472:2.480

Table 4 Number and percentage of successful solutions for each L.W. for case 5

L.W.	No.	Percentage	φ, deg
1	15	0.12%	144
2	12	0.07%	115
3	305	0.38%	51
4	11	0.08%	−66
5	14	0.09%	170
6	8	0.04%	161
7	98	0.19%	−142
8	250	0.34%	−136
9	6	0.05%	−83

A closer examination of which L.W.s yielded the most successful solutions produced some interesting results. Table 4 lists the number and the percentage of successful solutions for each L.W. For reference, the lunar phase angle φ for each launch window is also listed.

Table 4 clearly indicates that only L.W.s 3, 7, and 8 found a sufficient number of solutions to perform any meaningful analysis. The other L.W.s generally had far fewer trial solutions due to a narrower range of input parameters, and thus were hurt more by the coarseness of the grids used for case 5. In fact, L.W.s 3, 7, and 8 of case 5 all have approximately the same ranges for α, β, and Δv, and they correspond to the largest circles in Fig. 10 (L.W.s 6, 13, and 14). L.W.s 7 and 8 are about a month apart in launch time, while L.W. 3 is almost exactly a year before L.W. 8. These three launch windows had the lowest values for Δv and so had the lowest cost for leaving the moon.

Figure 13 zooms in on the two main regions of interest in Fig. 12—the dense cluster of fast-transfer solutions in the upper-left area, and the leftmost thick line in the lower-middle area.

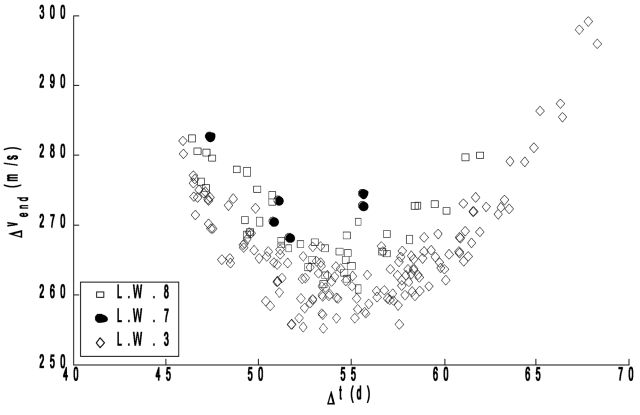

a) Fast-transfer solutions

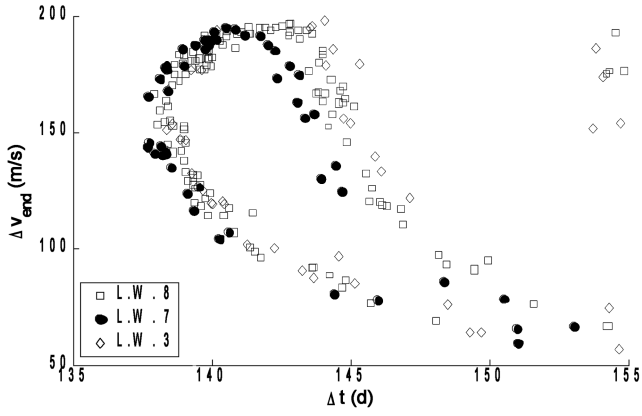

b) Slow-transfer solutions

Fig. 13 Two zoom-in regions from Fig. 12 for greater clarity.

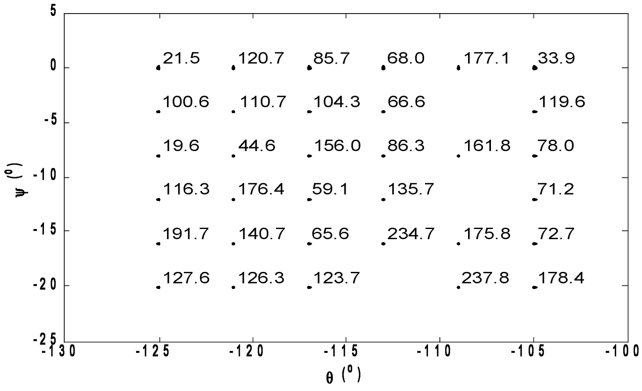

a) L.W. 7

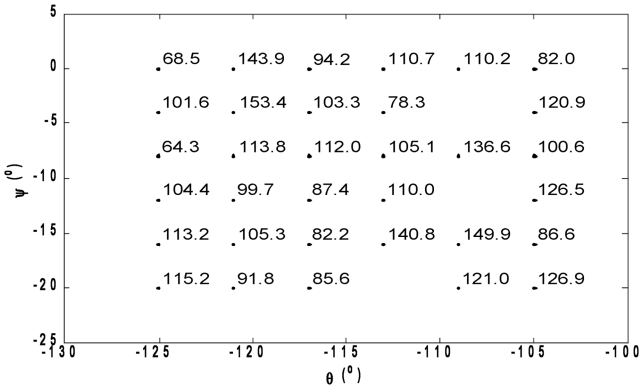

b) Average of all three L.W.s

Fig. 14 Minimum Δv_{end} (m/s) for each θ and ψ for case 5.

From Fig. 13, we can see that L.W. 3 has mostly higher Δv_{end} solutions, L.W. 7 has mostly lower Δv_{end} solutions, and L.W. 8 has a mix of both. Figure 14 examines the (θ, ψ) space by showing the lowest Δv_{end} at each point for L.W. 7 and for the average of the three launch windows examined.

Values for the lowest Δv_{end} range from 19.6 m/s to over 200 m/s. Three points in Fig. 14 could not reach L1 at all. For choosing a launch site, we notice that the lowest value for minimum Δv_{end} in both Figs. 14a and 14b occurs at $\theta = -125$ deg and $\psi = -8$ deg. The values for these angles indicate a launch site on the Earth-facing, trailing side of the moon, just south of the moon's orbital plane. Note, however, that this selection is somewhat arbitrary because the coarseness of the grid used in case 5 severely restricts the possibilities; for example, only midnight or noon launches were examined. However the ability to make a selection demonstrates the usefulness of the methods used in this paper.

Figure 15 shows the trajectory, plotted in the second reference frame, resulting in the lowest Δv_{end} for case 5, for which the parameters are $T = 1/21/2030$ 12:00, $\theta = -125$ deg, $\psi = -8$ deg, $\alpha = 74$ deg, $\beta = 44$ deg, and $\Delta v = 2.351$ km/s. In more conventional terms, these values for α and β correspond approximately to an azimuth of 44.9 deg and an elevation of 11.4 deg, while the launch time T indicates a launch at $\varphi = 34.9$ deg, between full moon and last quarter. The trajectory ended at L1 with an impulse of $\Delta v_{end} = 19.6$ m/s and a transfer time of 194 days.

In Fig. 15, the dark lines show the actual motion of the spacecraft and the moon, while the light lines represent the traces of the trajectory in the $x'y'$, $x'z'$, and $y'z'$ planes. As expected the spacecraft's motion is mostly planar, because it would require more energy and thus more Δv at each end of the trajectory to add any significant amount of out-of-plane motion. The spacecraft is launched from the moon, swings out until it is about twice as far from the Earth as the moon is, then swings back in within about 150,000 km of the Earth before shooting straight out to L1. No lunar flyby occurs for this trajectory.

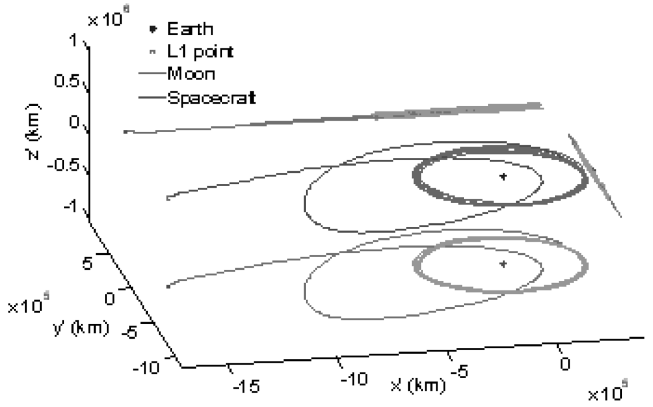

Fig. 15 Spacecraft trajectory for $T = 1/21/2030$ 12:00, $\theta = -125$ deg, $\psi = -8$ deg, $\alpha = 74$ deg, $\beta = 44$ deg, and $\Delta v = 2.351$ km/s resulting in $\Delta v_{end} = 19.6$ m/s and $\Delta t = 194$ days.

Although the results are not as detailed as would be required for actual mission design, the methods used were successful and should be applicable to a more detailed analysis. It was possible to locate a single launch site that could reach L1 with a low cost and has 3–4 day launch windows once or twice a year.

Direct numerical simulations were used in this paper as opposed to a more mathematically rigorous analytic approach such as dynamical systems theory (DST). Over the last two decades, Lagrange point missions have been studied using DST with a few missions flown. The Genesis spacecraft trajectory is an example of DST mission design where a trajectory was designed to travel to a sun–Earth Lagrange point, collect solar wind particles and safely return to them to Earth [9]. Many contributions have been made using DST for mission design, however, in many studies a more simple gravity model, such as the circular restricted three-body problem, is assumed [10]. This analysis modeled a more complex gravity field that resulted in the described numerical approach. Also, as the goal of this paper was to locate a single launch site on the moon rather than a single optimal trajectory, the numerical approach was deemed more appropriate for this case.

Conclusions

Simply getting to L1 from the moon is not a difficult problem. Getting there quickly and cheaply is also relatively easy—as long as one could control the initial conditions to several decimal places. Because a highly sensitive trajectory would likely result in more and larger course corrections, it was determined that a truly optimal trajectory would have not only a low cost but a low sensitivity as well.

Solving the full forward problem was complicated because hitting a point in 3-D space is nearly impossible for random initial conditions. The reverse model in this case was able to locate a high-density region of solutions with launch windows approximately 3 weeks to 6 months apart over a 2-year period. It was possible to identify a single optimal launch site that could reach L1 with a low fuel cost and launch windows approximately 3–4 days long that occur one or twice a year to within the resolution of the solution space. Running a more refined grid for this data would likely result in lower fuel costs and more available launch windows.

References

[1] Angel, R., "Feasibility of Cooling the Earth with a Cloud of Small Spacecraft Near the Inner Lagrange Point (L1)," *Proceedings of the National Academy of Sciences of the United States of America*, Vol. 103, No. 46, Nov. 2006, pp. 17184–17189.

[2] Farquhar, R. W., "The Flight of ISEE-3/ICE: Origins, Mission History, and a Legacy," *Journal of the Astronautical Sciences*, Vol. 49, No. 1, Jan.–March 2001, pp. 23–73.

[3] Dunham, D. W., and Roberts, C. E., "Stationkeeping Techniques for Libration-Point Satellites," *Journal of the Astronautical Sciences*, Vol. 49, No. 1, Jan.–March 2001, pp. 127–144.

[4] Christian, E. R., and Davis, A. J., "ACE Mission," http://www.srl.caltech.edu/ACE/ace_mission.html [retrieved 13 Nov. 2007].

[5] Lo, M., Williams, B. G., Bollman, W. E., Han, D., Hahn, Y., Bell, J. L., Hirst, E. A., Corwin, R. A., Hong, P. E., Howell, K. C., Barden, B., and Wilson, R., "Genesis Mission Design," *Journal of the Astronautical Sciences*, Vol. 49, No. 1, Jan.–March 2001, pp. 145–167.

[6] Prussing, J. E., and Conway, B. A., *Orbital Mechanics*, Oxford Univ. Press, Oxford, England, U.K., 1993, pp. 3–9.

[7] Yeomans, D. K., and Chamberlin, A. B., "HORIZONS Web-Interface," http://ssd.jpl.nasa.gov/horizons.cgi [retrieved 13 Nov. 2007].

[8] Matlab R2006a, The Mathworks, "Matlab Function Reference: ode23, ode45, ode113, ode15s, ode23s, ode23t, ode23tb," http://www.mathworks.com/access/helpdesk/help/techdoc/ref/ode23.html [retrieved 13 Nov. 2007].

[9] Howell, K. C., Barden, B., and Lo, M., "Application of Dynamical Systems Theory to Trajectory Design for a Libration Point Mission," *Journal of the Astronautical Sciences*, Vol. 45, No. 2, 1997, pp. 161–178.

[10] Baoyin, H., and McInnes, C., "Trajectories to and from the Lagrange Points and the Primary Body Surfaces," *Journal of Guidance, Control, and Dynamics*, Vol. 29, No. 4, 2006, pp. 998–1003.